

Graphene Oxide-Loaded Zinc Phosphate as an Anticorrosive Reinforcement in Waterborne Polyurethane Resin

Youtong Wu¹, Shaoguo Wen^{2,*}, Jihu Wang², Guangyu Wang², Kai Sun²

College of Chemistry and Chemical Engineering, Shanghai University of Engineering Science, Shanghai 201620, PR China

*E-mail: sgwen1@sues.edu.cn

Received: 15 January 2019 / Accepted: 13 March 2019 / Published: 10 May 2019

Graphene oxide zinc phosphate (GO-ZP) composites were synthesized by a one-step ultrasonic wave-assisted method and then incorporated into waterborne polyurethane as the anticorrosive reinforcement to produce graphene oxide zinc phosphate/polyurethane (GO-ZP/PU) composites. The GO-ZP composites were characterized by Fourier transform infrared spectroscopy (FTIR), X-ray diffraction (XRD), X-ray photoelectron spectroscopy (XPS), scanning electron microscopy (SEM) and transmission electron microscopy (TEM). The anticorrosive properties of the GO-ZP-reinforced PU composite coatings were characterized by potentiodynamic polarization and electrochemical impedance spectroscopy (EIS). The correlations among the mass ratio of GO to Zn₃(PO₄)₂, the concentration of GO-ZP added to the waterborne polyurethane (WPU) and the anticorrosive properties of the composites were investigated. The results showed that excellent anticorrosive properties were achieved for the GO-ZP/PU composite with the 0.5 wt% GO-ZP (3:1) coating, which had a corrosion current density (i_{corr}) of only 4.41×10^{-7} A/cm² and a charge transfer resistance (R_{ct}) of 1.104×10^4 Ω cm².

Keywords: graphene oxide, zinc phosphate, waterborne polyurethane, coating, corrosion resistance

1. INTRODUCTION

The corrosion of low-carbon steels is one of the most important issues in many fields, so it is of great importance to prevent steel corrosion. Many effective methods have been developed to improve the anticorrosion performance of steel, but the most valid way to protect steel is to use a coating with anticorrosive fillers [1, 2]. However, traditional anticorrosive coatings are mostly based on solvents and toxic heavy metals such as lead and chromium that release volatile organic compounds and affect human health and the environment [3]. With the popularity of environmentally friendly water-based coatings, solvent-based coatings are gradually being replaced. Nevertheless, there are many limitations for water-based coatings, such as poor crosslinking density, that affect their corrosion resistance and durability. In

In addition, there are many defects on the surface of coatings that affect their anticorrosive ability and allow corrosive media to easily reach the substrate. Many studies have been conducted to improve the corrosion resistance of coatings, and the addition of a corrosion inhibitor is an effective approach [4-6]. In general, inorganic materials were added into a polymer matrix to attain cooperative properties. Water-borne polyurethanes have the characteristics of wear resistance, excellent flexibility, glossiness, general chemical stability, good weather fastness and low volatile organic compound content. It is a typical comprehensive polymer material in industry [7-10]. However, the adhesion and bubbling ability of the film is poor, resulting in corrosion of the steel matrix, which affects the application of water-borne polyurethanes as a low carbon steel protective coating.

Graphene oxide is an important material because of its two-dimensional layered structure, which has the nature of its potentially scalable precursor of graphene [11, 12]. A variety of functional groups on the surface of graphene enable compatibility with base materials [13]. As a new material, exfoliated graphene not only has good electrical conductivity but also has a large specific surface area, so it has the potential for electric energy storage and barrier properties [14-19]. It has been reported that graphene oxide and graphene derivatives have been successfully applied in polymers as functional pigments, such as anticorrosion reinforcements and flame retardants [20-23]. A recent study by Jian Luo involved reduced sulfonated graphene (RSG) as an anticorrosive filler added to waterborne polyurethane to reinforce corrosion resistance [24]. Moreover, the oxygenated groups on the sheet could load functional materials and serve as nucleation centers for crystallization [25]. Graphene oxide is usually prepared by Hummers method, but ultrasonication is required before using, which can cause defects on the surface and affect the barrier properties [26].

Zinc phosphate is a multifunctional material with different morphologies and crystal structures that can be applied in many different fields [27, 28]. The introduction of nontoxic zinc phosphate as a corrosion inhibitor has achieved notable results. Moreover, phosphate can improve the adhesion of organic polymer coatings. In a previous study, zinc phosphate was modified to increase its solubility and reduce the phosphating time to improve the corrosion resistance of coating systems [29]. To the best of our knowledge, the preparation of traditional phosphating films require a great deal of energy and is time consuming [30, 31]. In addition, zinc phosphate as an anticorrosive pigment has many shortcomings in industrial applications, such as insufficient anticorrosion efficiency. In previous studies, researchers modified zinc phosphate to increase its solubility and reduce the time of inhibitor film formation to improve the corrosion resistance of coating systems [32, 33]. Dagdag O. added zinc phosphate to an epoxy resin, which was synthesized by diglycidyl ether 4,4-dihydroxy diphenyl sulfone (DGEDDS) to improve corrosion resistance [34]. However, the solvent-based resin still had certain environmental problems, and waterborne polyurethane still had some shortcomings in anti-corrosion performance.

In this study, we used graphene oxide to load zinc phosphate to reduce its surface defects and improve the corrosion resistance of the zinc phosphate system. We focused on the influence of the GO ratio on the composites and the cooperation of the composites with waterborne polyurethane resin on the substrate. The graphene oxide zinc phosphate (GO-ZP) composites were synthesized by a one-step ultrasonic wave-assisted precipitation method, and the effects of different proportions of GO-ZP composites on the anticorrosion performance of coatings were evaluated by electrochemical data. The data showed that the GO-ZP/WPU composite coating possessed a better corrosion resistance than that

of the GO/phosphate coating [35], and lower corrosion current value than RSG composites coating [24]. The morphology and crystal composition of the composites were investigated by transmission electron microscopy (TEM) and X-ray diffraction (XRD).

2. MATERIALS AND METHODS

2.1 Materials

Nanographite powder particles were obtained from Shanghai Humai Composite Materials Co. LTD (China). The waterborne polyurethane resin (WPU) and waterborne dispersant KY922 were supplied by Shanghai Huayi Fine Chemical Co. LTD (China). Potassium permanganate (KMnO_4), sodium phosphate dibasic ($\text{Na}_2\text{HPO}_4 \cdot 12\text{H}_2\text{O}$), sodium nitrate (NaNO_3), Sodium chloride (NaCl), zinc phosphate (ZP) and hydrogen peroxide (H_2O_2 , purity of 33%) were reagent grade and purchased from Aladdin Biochemical Technology Co. LTD (China). Zinc acetate dehydrate, concentrated sulfuric acid (98%), hydrochloric acid (5 wt%), and ammonium hydroxide and ethanol (95%) were analytical grade and obtained by Sino Pharm Chemical Reagent Co. LTD (Shanghai, China). Distilled water was used in all of the experiments, and all reagents were used as received.

2.2 Preparation of graphene oxide

Graphene oxide (GO) was synthesized by a modification of Hummers method [36], where 3 g of oxidic graphite powder and 1.5 g of sodium nitrate (ratio 2:1) were added into a certain amount of H_2SO_4 in a 150 ml flask. The flask was put into an ice bath, followed by the addition of 9 g of KMnO_4 . The resultant mixed solution was heated to 40°C under mechanical stirring. After 30 min, 90 ml distilled water was slowly dropped into the mixture below 90°C , and 40 ml H_2O_2 (diluted to 25%) was added to the flask after 1~1.5 h. Upon completion of the reaction, the homogeneous brown dispersion was centrifuged and washed with hydrochloric acid (5 wt%) to remove the metallic ions, then washed with deionized water at $\text{pH} = 7$ and vacuum-dried 24 h at 60°C in a vacuum oven.

2.3 Synthesis of GO/zinc phosphate

The graphene oxide zinc phosphate (GO-ZP) composites were synthesized by a one-step ultrasonic wave-assisted precipitation method with [37, 38]. In this method, 30 mg graphene oxide was considered as 1 proportion, and 0.01 mol zinc phosphate was considered as 1 proportion. The ratios of GO-ZP were 1:1, 3:1 and 5:1, and were named as GO-ZP (1:1), GO-ZP (3:1) and GO-ZP (5:1), respectively. First, 0.04 mol sodium phosphate dibasic ($\text{Na}_2\text{HPO}_4 \cdot 12\text{H}_2\text{O}$) was put into 40 ml distilled water with sufficient stirring. Then, the as-prepared GO sheets were exfoliated by an ultrasonic cell crusher at a power of 150 W for 1 h in 100 mL water and 20 mL ethanol solution. After that, the processed GO dispersion was added into $\text{Na}_2\text{HPO}_4 \cdot 12\text{H}_2\text{O}$ aqueous solution with continuous stirring and heated to 40°C . Then, 0.03 mol zinc acetate was dissolved in a certain amount of water and added into the mixture

slowly with ultrasonic irradiation (ACE horn, 30 kHz frequency) for 30 min. The pH was adjusted to 8~10 by controlling the addition of aqueous ammonium hydroxide. In the initial reaction, when the zinc acetate solution was added, a large number of flocculent complexes were generated in the solution, and as the amount of zinc ions increased, the flocs gradually vanished. The flask was heated in a water bath at 80°C for 1 h and adjusted to 50°C for 3 h. Then, the specimens were separated via centrifugal machine and washed several times with deionized water until the pH was 7. Finally, the sample was dried at 60°C in an air blowing thermostatic oven.

2.4 Preparation of GO-ZP/WPU composites

Samples with different contents of GO-ZP and ZP were named as GO-ZP (x:1)-0.1wt%, 0.5wt%, 1wt%, and were gradually added into a 30 g WPU resin with 38.61 mg dispersant and stirring at 300 rpm for 2 h. Subsequently, the GO-ZP/WPU mixtures were painted on a steel substrate by a bar coater and cured at room temperature (25°C) for 4 days. The detailed production process is shown in Table 1. The thickness of the composite coating tested was controlled to $30 \pm 5.5 \mu\text{m}$.

Table 1. The formulation of the GO-ZP/WPU composite coating

Sample name	Graphene oxide /mg	Sodium phosphate dibasic /g	Zinc acetate /g	Waterborne dispersant /mg
Zinc phosphate	0	14.32	6.58	38.61
GO-ZP (1:1)	30	14.32	6.58	38.61
GO-ZP (3:1)	90	14.32	6.58	38.61
GO-ZP (5:1)	150	14.32	6.58	38.61

2.5 Characterization

The crystal structure of the powder was determined by X-ray diffraction (Brook Co., Germany) with a copper $K\alpha$ radiation source ($\lambda=0.15406 \text{ nm}$). Fourier transform infrared spectroscopy (FTIR) spectra of composites were obtained on a L160-8000 spectrometer (PerkinElmer, USA). X-ray photoelectron spectroscopy (XPS) measurements were carried out on a Thermo ESCALAB 250XI equipped with an Al $K\alpha$ X-ray source. The morphology of the sample was observed by scanning electron microscopy (SEM, Hitachi Co., SU8010, Japan) and transmission electron microscopy (TEM, JEOL, JEM-2000, Japan). All electrochemical measurements were performed on an electrochemical workstation (CHI660E, Shanghai Chenhua Device Co., China) at room temperature and utilized a platinum electrode and calomel electrode to obtain potentiodynamic polarization data. A voltage range from -0.8 V to -0.1 V, frequency range from 100000 Hz to 0.01 Hz, and scan rate of 1 mV/s were used. A 3.5 wt% NaCl solution was used as the electrolyte. The pH value was measured by using a pH meter (Shanghai Yidian Scientific Instrument Co.). Finally, the thickness of films was determined by a coating thickness gauge, and bar coaters were supplied by Guangzhou Guoou Electronic Technology Co., China.

3. RESULTS AND DISCUSSION

3.1 Characterizations of graphene oxide/zinc phosphate (GO-ZP) composites

The surface chemical structures of GO, ZP and GO-ZP were analyzed by Fourier transform infrared spectroscopy. As shown in Fig. 1 (a), the ZP spectrum displayed characteristic peaks at 942-1200 cm^{-1} and 500-700 cm^{-1} for more than one stretching vibration and bending vibration absorption from the PO_4^{3-} groups [39]. The formation of hydroxide groups (-OH) was confirmed by the appearance of the stretching vibration band at 3426 cm^{-1} for the GO spectrum. Moreover, the two strong absorption peaks at 2920 cm^{-1} were attributed to the stretching vibration of C-H groups. The weak peak at approximately 1622 cm^{-1} was believed to be the result of the C=C stretching vibrations, which manifested the GO carbon backbone as a sheet in reaction [40]. Fig. 1 (b) presents the FTIR spectra of GO-ZP (1:1), GO-ZP (3:1) and GO-ZP (5:1). The strong peak at 3402 cm^{-1} revealed that some -OH groups were associated with unbound water. The absorption peak at approximately 1644 cm^{-1} was associated with the bending vibration absorption peaks of water molecules, which indicated that water crystals existed in the samples. All the spectra verified that the samples contained zinc phosphate and that the PO_4^{3-} groups had more than one stretching vibration and bending vibration.

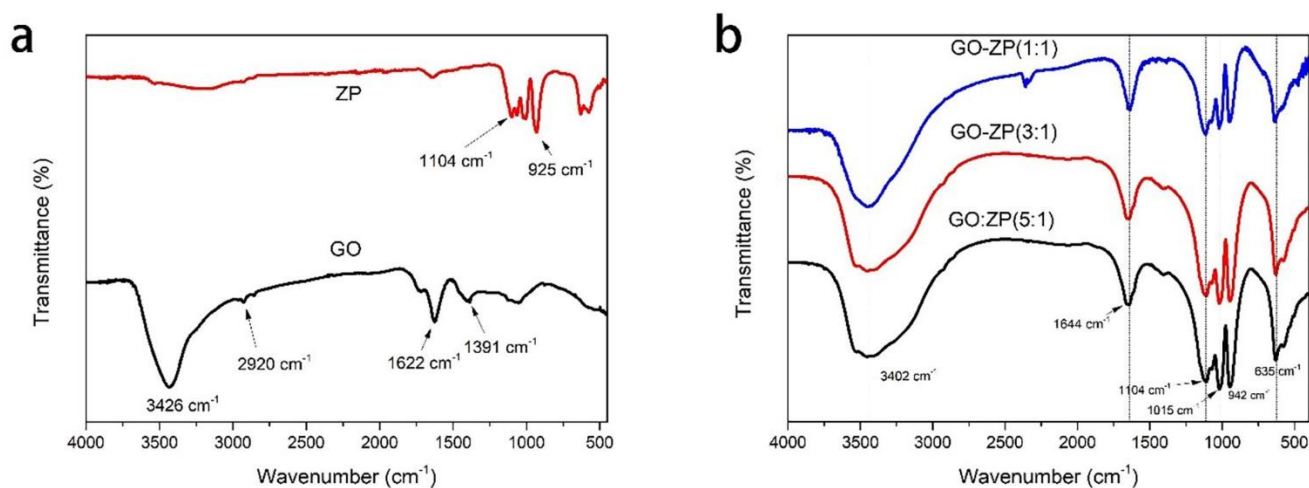


Figure 1. FTIR spectra of ZP, GO, GO-ZP (1:1), GO-ZP (3:1) and GO-ZP (5:1).

The surface element content and chemical state of the composites were investigated by X-ray photoelectron spectroscopy (XPS). As shown in Fig. 2, the XPS survey spectrum demonstrated the presence of Zn, P, C and O. The C 1s peaks in Fig. 3 (a) consisted of 4 peaks that fit Gaussian peaks centered at 284.6, 285.4, 286.4 and 288.6 eV, which belonged to C=C, C-C, C-O and C(O)O, respectively. The peaks at 531.3 and 532 eV in Fig. 3 (b) can be attributed to the hydroxide component and O-P-O bonding, respectively. As shown in Fig. 3 (c) and (d), the peaks at 133.4 eV ($\text{P } 2p_{1/2}$) and 134.2 eV ($\text{P } 2p_{2/3}$) were assigned to the O-P-O bonding in the (PO_4^{3-}) network [41]. As shown in Fig. 3 (d), the two peaks at 1045.6 eV and 1022.6 eV were attributed to Zn $2p_{1/2}$ and Zn $2p_{3/2}$, respectively [42]. According to the above XPS spectra, the GO-ZP materials were prepared in this study.

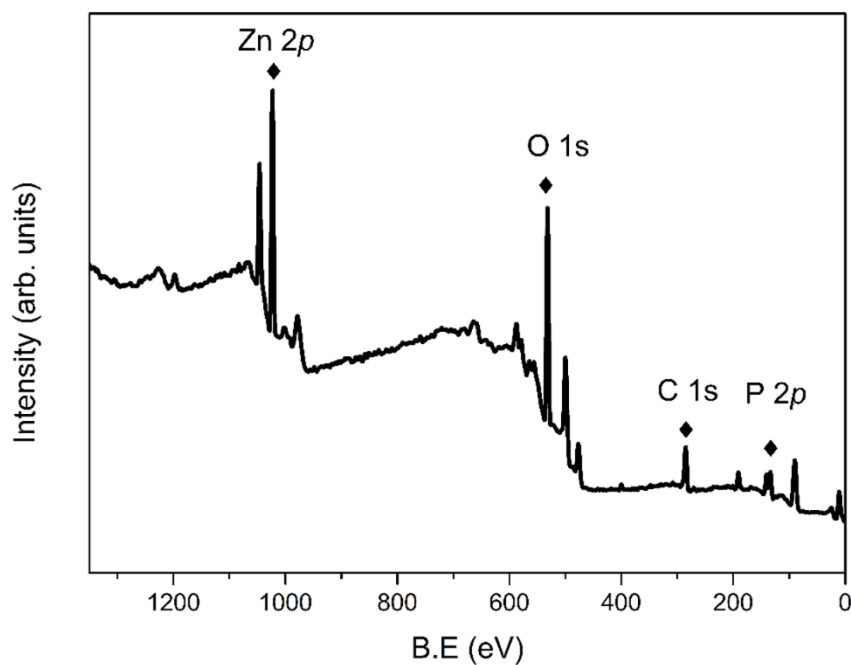


Figure 2. XPS spectra of the GO-ZP (x:1) sample

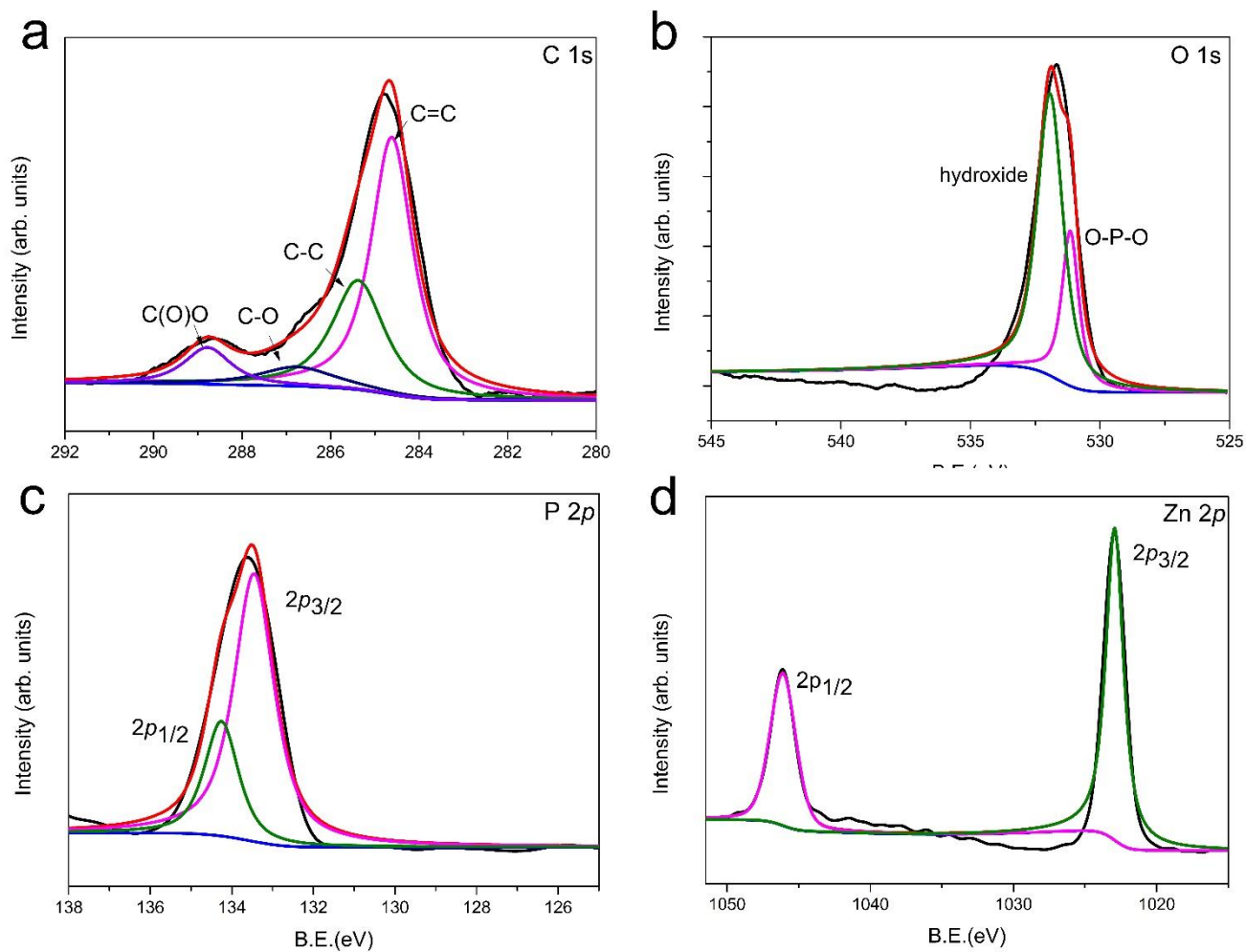


Figure 3. XPS spectra of carbon (a) C 1s, (b) O 1s, (c) P 2p and (d) Zn 2p.

The XRD patterns of the prepared GO and GO-ZP with different qualitative concentrations (GO-ZP (1:1), GO-ZP (3:1) and GO-ZP (5:1)) are presented in Fig. 4. All synthesized hybrids indicated the presence of $\text{Zn}_3(\text{PO}_4)_2 \cdot 4\text{H}_2\text{O}$ (Hopeite, JCPD file #76-0896, lattice constant: $a=10.597 \text{ \AA}$ $b=18.318 \text{ \AA}$ $c=5.031 \text{ \AA}$). As shown in Fig. 4 (b), a reflection peak at approximately 10.8° corresponds to the successful formation of graphite oxide with an interlayer spacing of 0.813 nm . The diffraction patterns of the prepared GO-ZP samples indicated that most diffraction peaks corresponded to the PDF of standard zinc phosphate. The zinc phosphate had diffraction peaks at 9.6° , 17.4° , 19.4° , 26.3° , 31.3° and 46.8° 2θ , which correspond to the crystal planes of (020), (210), (040), (221), (241), (151) and (281) of the orthorhombic system, respectively. The average lattice constants were $a=10.6841 \text{ \AA}$, $b=18.4218 \text{ \AA}$, and $c=5.0497 \text{ \AA}$, which are similar to the standard material. A comparison of the different ratios of GO-ZP composites and patterns with an increase in the addition of GO mass indicated that the crystallinity clearly decreased in terms of the (020) and (040) peak intensities. The addition of graphene did not affect the composition of the complex, but it can change the growth orientation of the phosphate crystals [35]. In addition, the results suggested that the crystallinity of these composites decreased with increasing graphene oxide loading, which was indicated in the decreasing peak intensities.

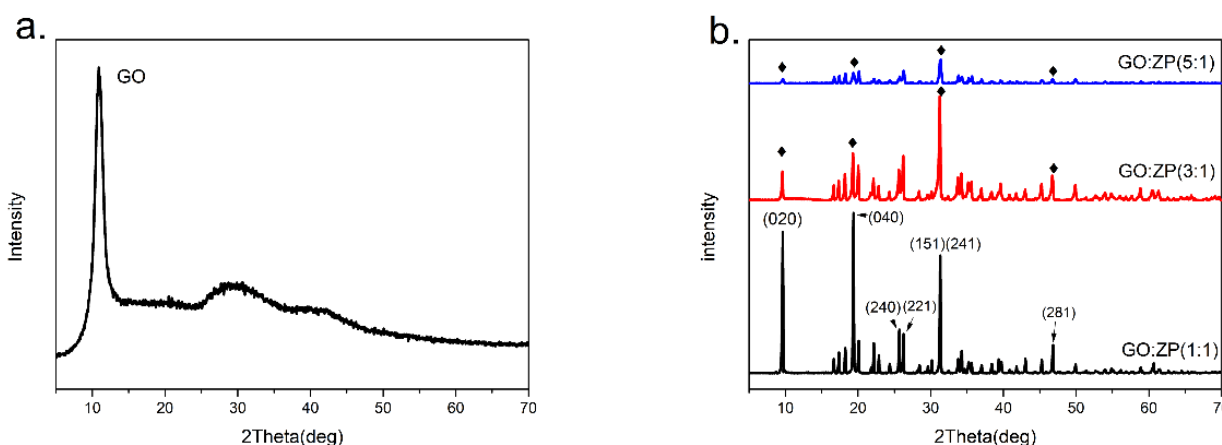


Figure 4. XRD pattern (a) of GO. XRD patterns (b) of GO-ZP (1:1), GO-ZP (3:1) and GO-ZP (5:1).

Previous studies showed that zinc phosphate tends to form flakes in acidic conditions [43, 44]. Fig. 5 shows the size and morphology of the prepared product. As shown in Fig. 5 (a-c), as the GO mass increased, the average cross-section dimension of zinc phosphate decreased. Most composites presented irregular flake crystals, but a few showed sheet-like rectangles with an average thickness of $1\sim 1.5 \mu\text{m}$. In Fig. 5 (a), the crystals appeared as blocks and clusters. As shown in Fig. 5 (b) and (c), the prepared materials had a flat sheet morphology. In contrast with GO-ZP (1:1), the average transverse dimension of the GO-ZP (3:1) hybrid was less than $5 \mu\text{m}$, and the cross-sectional size decreased from 6 to $1 \mu\text{m}$. It can be seen clearly from Fig. 5 (c) that most particles decreased in size (approximately $1\sim 2 \mu\text{m}$) when the ratio of the GO-ZP composites arrived at 5:1. It is worth noting that the thickness of the materials increased, which could be attributed to the growth points provided by the thin layers of graphene for the crystallization of the ZP to form a sandwich structure [45]. Compared with the pure zinc phosphate in

Fig. 3 (d), the modified composites showed an irregular crystal shape, which could be attributed to the acoustic cavitation effect of ultrasound on the crystal formation. At the beginning of the reaction, zinc ions were adsorbed on the graphite oxide sheets through coordination interactions with the C-C and -OH species or an ion-exchange with H⁺ from carboxyl, which caused the amount and properties of charges on GO sheets to vary [46]. In this system, the solute molecules had sufficient energy and speed due to the oscillation and cavitation mechanisms, which increased the probability of collision between molecules and the static liquid layer passing through the crystal surface [47, 48]. On the one hand, the effect of ultrasonic waves was effective in reducing the size of the substances and led to small and uniform crystals [49]. On the other hand, the ultrasonic waves promoted the mixing of the solution and the amount of local nucleation under controlled conditions, which decreased the possibility of excessive crystal aggregation [50].

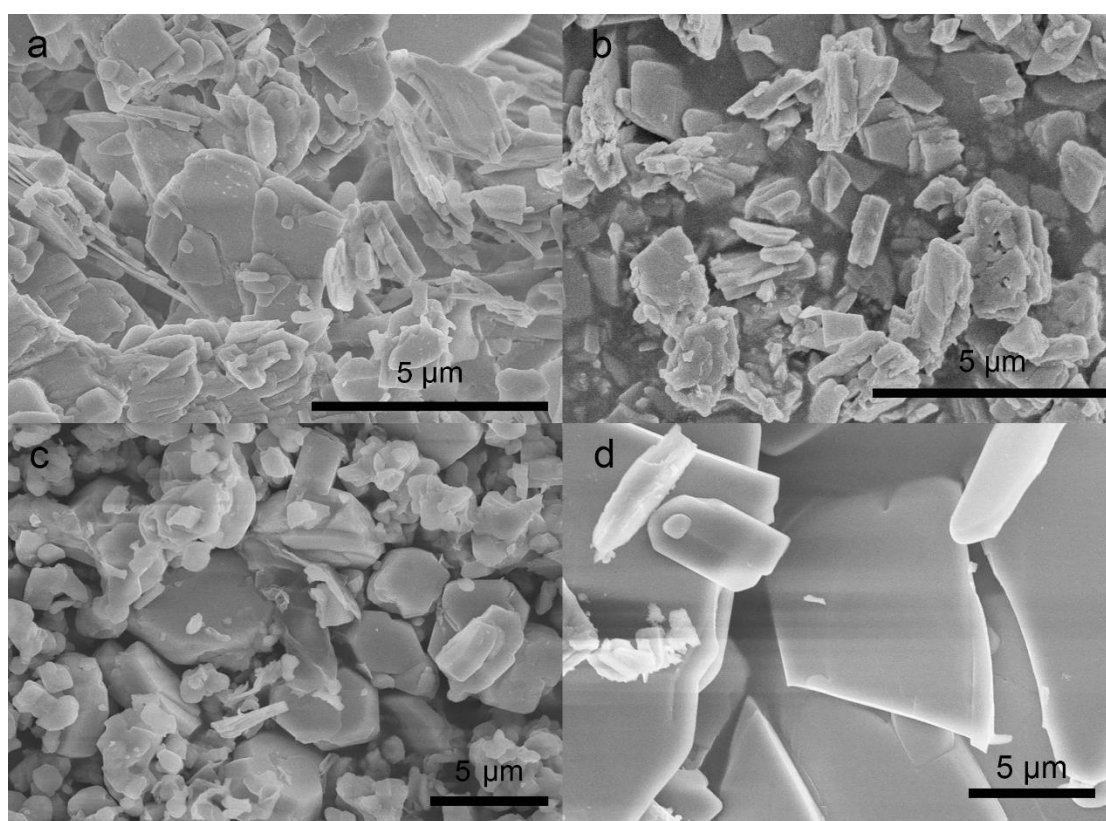


Figure 5. SEM image of GO-ZP with different ratios of GO and ZP: (a) 1:1, (b) 3:1, (c) 5:1 and (d) pure zinc phosphate.

As seen in the TEM images, zinc phosphate was successfully loaded onto GO flakes. The TEM images in Fig. 6 (a) show that the zinc phosphate grew on the GO sheets uniformly and exhibited a corrugated and transparent sheet-like structure at the edges of the composites, indicating that the GO and zinc phosphate were most likely combined by van der Waals interactions [34]. Moreover, the size of the complex particles was 1.5 μm. As shown in Fig. 6 (b), the sandwich structure can be observed clearly. The GO-ZP (3:1) composites exhibited an overlapping thinner flake with a transverse dimension of 1

μm . The phosphate crystals were deposited on the GO sheets, which indicated that the functional groups on the GO could serve as active sites for nucleation of phosphate crystals (Fig. 7).

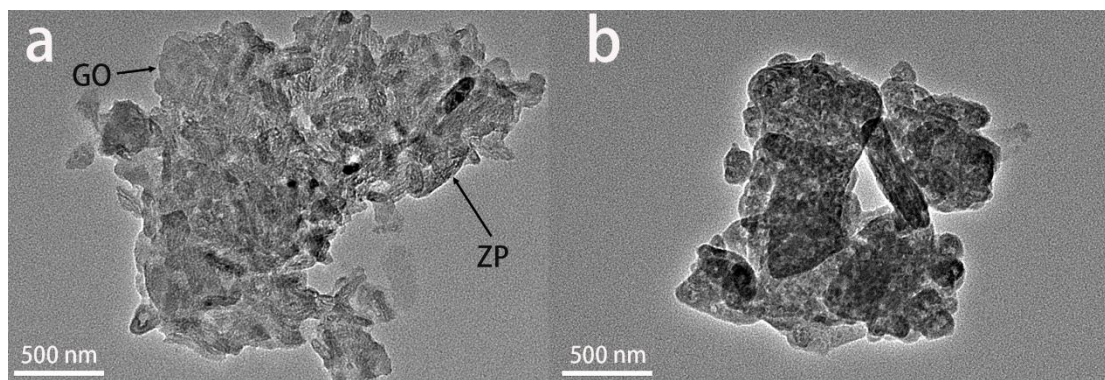


Figure 6. TEM images of GO-ZP composites with a mass ratio of 3:1.

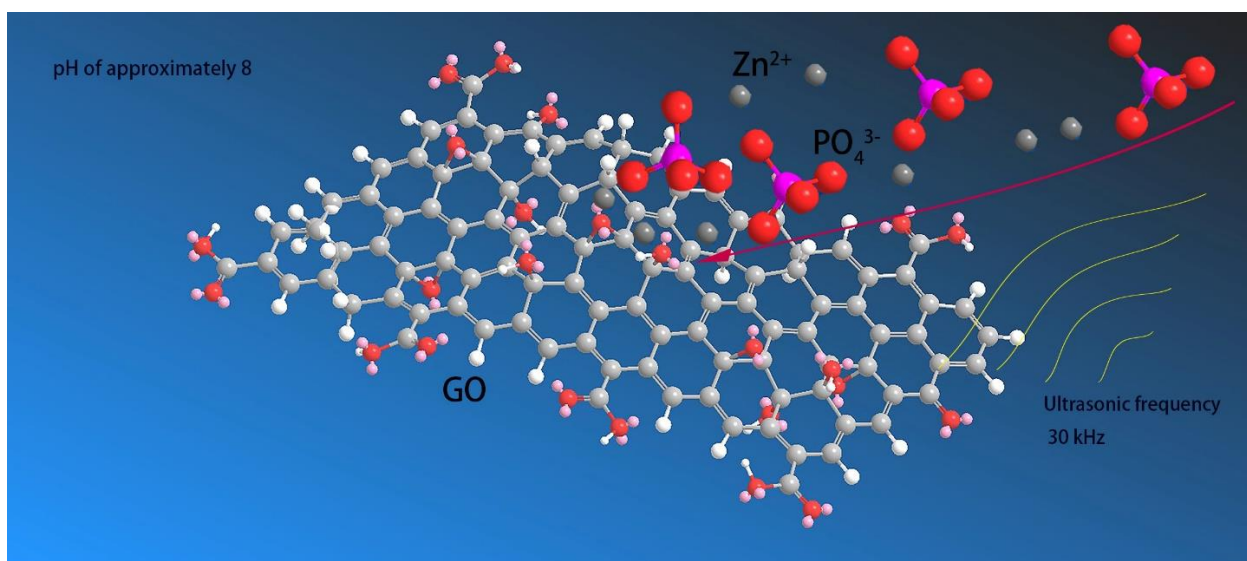


Figure 7. The formation of GO-ZP composites.

3.2 Corrosion measurements

Potentiodynamic polarization curves and electrochemical impedance spectroscopy are common methods for characterizing the corrosion behavior of metals. In this study, corrosion current density (i_{corr}), corrosion potential (E_{corr}), corrosion rate (CR) and protection efficiency (η) were used to investigate the anticorrosive effect of the GO-ZP composites.

$$\eta (\%) = 100\% \times \left(1 - \left(\frac{i_{\text{corr},i}}{i_{\text{corr},b}} \right) \right) \quad \text{Eq.1}$$

In the equation (1) $i_{\text{corr},i}$ and $i_{\text{corr},b}$ values are corrosion current densities of the samples in the corrosive solution with and without the pigment extract, respectively.

As shown in Fig. 8 and Table 2, the polarization curve of the low carbon steel after immersion for 8 h in 3.5 wt% NaCl solution showed that the polarization current density of the GO-ZP hybrid coating was only 2 orders of magnitude lower than that of bare steel sheets. For the same ratio, the corrosion current of the composite GO-ZP (1:1)-0.5 wt% (1.88×10^{-6} A/cm²), GO-ZP (3:1)-0.5 wt% (4.41×10^{-7} A/cm²) and GO-ZP (5:1)-0.5 wt% (2.73×10^{-6} A/cm²) were less than that of pure zinc phosphate (5.54×10^{-6} A/cm²). The results indicated that the composites with a small particle size benefitted the dispersion of the system and blocked micropores to prevent the corrosive medium from penetrating the steel surface.

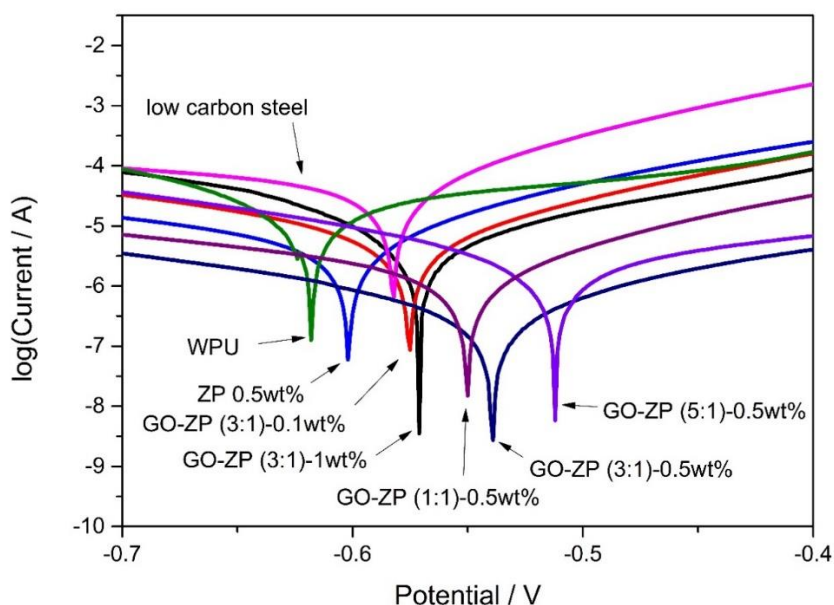


Figure 8. Potentiodynamic polarization curves of low carbon steel, WPU, ZP 0.5wt% and different mass ratio of GO-ZP (x:1) composites coating after immersion for 8 h in 3.5 wt% NaCl solution at pH=7.

The smallest i_{corr} was obtained for GO-ZP (3:1)-0.5 wt% (4.41×10^{-7} A/cm²), as shown in Table 2, indicating the best corrosion inhibitive performance for this sample. Compared with the ZP specimen and pure WPU coating, as the GO content increased, the number of GO-ZP composites increased gradually, the Tafel curves of all composites moved to the right, and the E_{corr} showed more positive data points. Moreover, as shown in the table, the protection efficiency (η) value of the GO-ZP (3:1)-0.5 wt% sample increased by at least 99%. Compared with other samples, the GO-ZP composites coating showed a preferable improvement of η . The result of potentiodynamic polarization curves indicated that the introduction of graphene effectively improved the corrosion resistance of the zinc phosphate corrosion inhibitor.

The equivalent circuit diagram is shown in Fig. 10, where R_s is the solution resistance, R_{ct} is the charged transfer resistance, CPE is the constant phase element. The corrosion rate increases as R_{ct} declines. The impedance of the CPE is expressed as Eq. 2 [51]:

$$Z_{\text{CPE}} = [f_0 (j\omega)^n]^{-1} \quad \text{Eq. 2}$$

where f_0 is a proportionality coefficient, w is the angular frequency, and j is the imaginary number. Meanwhile, the electrolyte is closely related to permittivity in metaphase and anaphase of corrosion, leading to an increase in CPE, which can contribute to the diffusion of the electrolyte.

Table 2. Electrochemical measurement data after immersing 8 h in NaCl 3.5 wt% solution pH=7

Samples	E_{corr} (mV)	i_{corr} (A/cm ²)	b_a (mV/dec)	b_c (mV/dec)	μ (g·m ⁻² ·h ⁻¹)	η (%)
Low carbon steel	-582	4.94×10^{-5}	89	-317	5.14×10^{-1}	
WPU	-618	2.42×10^{-5}	280	-128	2.51×10^{-1}	51%
ZP (0.5%)	-602	5.54×10^{-6}	94	-208	5.76×10^{-2}	89%
GO-ZP (1:1)-0.5 wt%	-550	1.88×10^{-6}	109	-229	1.95×10^{-2}	96%
GO-ZP (3:1)-0.5 wt%	-539	4.41×10^{-7}	134	-169	4.51×10^{-3}	99%
GO-ZP (5:1)-0.5 wt%	-512	2.73×10^{-6}	209	-140	2.83×10^{-2}	94%
GO-ZP (3:1)-0.1 wt%	-575	6.88×10^{-6}	116	-166	7.15×10^{-2}	86%
GO-ZP (3:1)-1 wt%	-571	5.96×10^{-6}	143	-940	6.19×10^{-2}	88%

E_{corr} : corrosion potential, i_{corr} : corrosion current density, μ : corrosion rate, η : protection efficiency, b_a : anodic Tafel slope, b_c : cathodic Tafel slope

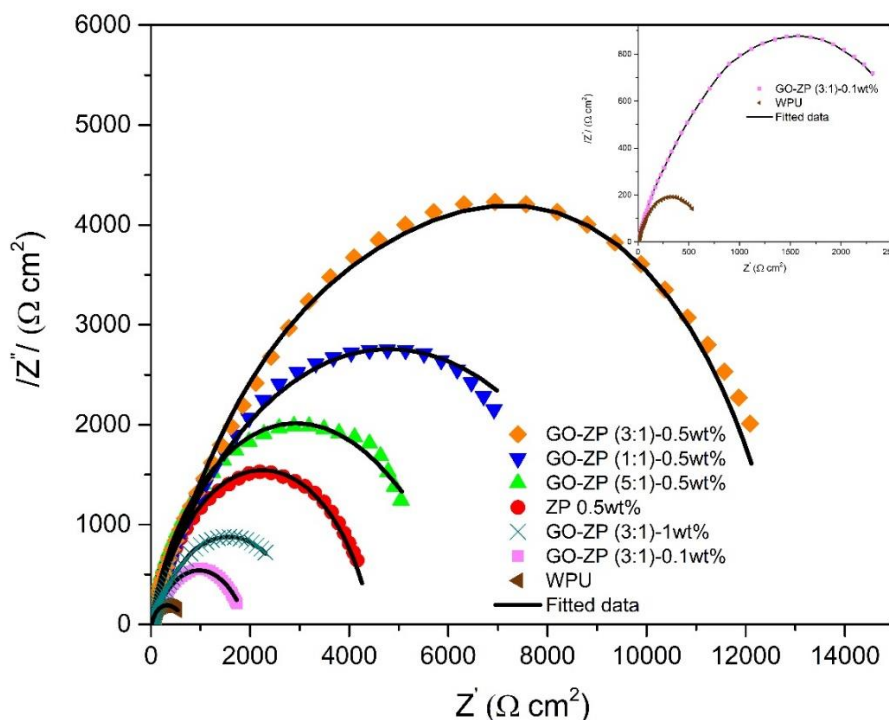


Figure 9. EIS plots of WPU, ZP 0.5 wt% and different mass ratio of GO-ZP (x:1) composites coating after immersion for 8 h in 3.5 wt% NaCl solution at pH=7

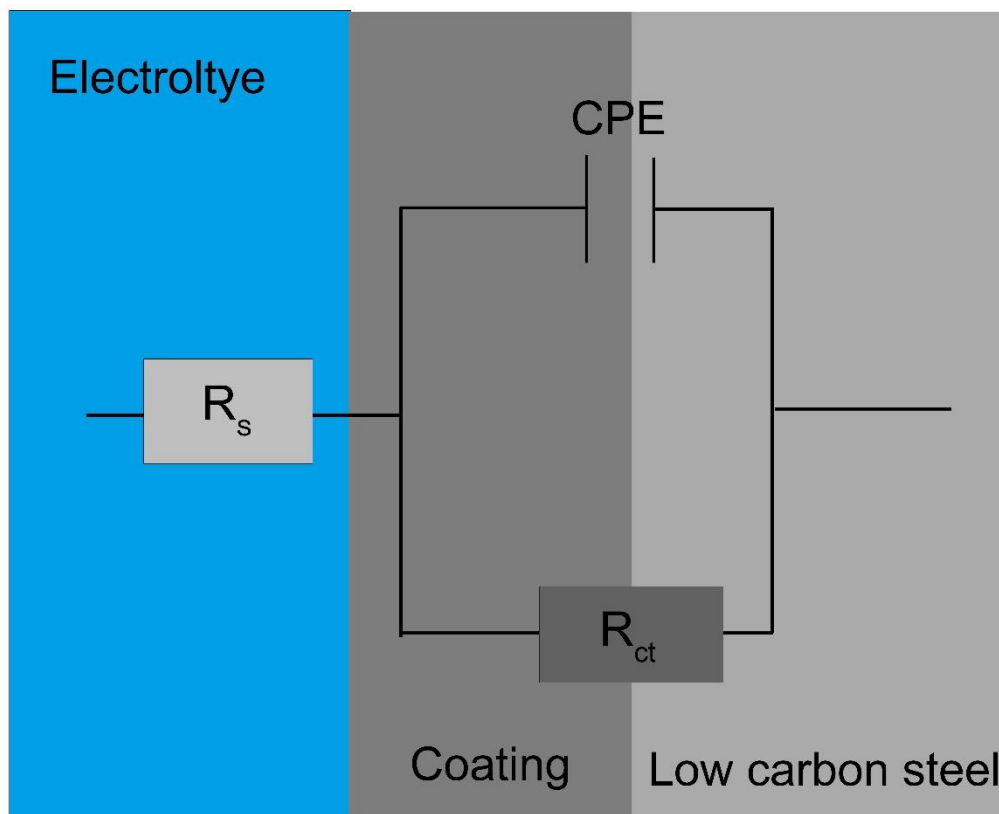


Figure 10. The proposed equivalent electrical circuit according to the impedance data.

Table 3. EIS data for different composite coatings

Sample name	R_s ($\Omega \text{ cm}^2$)	R_{ct} ($\Omega \text{ cm}^2$)	CPE
WPU	15.12	826	3.635×10^{-4}
ZP 0.5wt%	18.42	3762	6.996×10^{-5}
GO-ZP (1:1)-0.5 wt%	16.52	6324	3.647×10^{-5}
GO-ZP (3:1)-0.5 wt%	18.14	11040	9.841×10^{-6}
GO-ZP (5:1)-0.5 wt%	17.21	4726	5.141×10^{-5}
GO-ZP (3:1)-0.1 wt%	16.80	1515	8.945×10^{-5}
GO-ZP (3:1)-1 wt%	14.12	2231	7.176×10^{-5}

R_s -solution resistance, R_{ct} -charged transfer resistance, CPE-constant phase element

The film formation can be characterized by the deposition of the inhibitive species released from the sample as the following reaction:



Therefore, the formation of protective films occurred via complex chemical and electrochemical processes. The film of the inhibitor deposited as a barrier at the anode and cathode locations to prevent the corrosion medium from diffusing through the defects to the metal surface, as shown in Fig. 11.

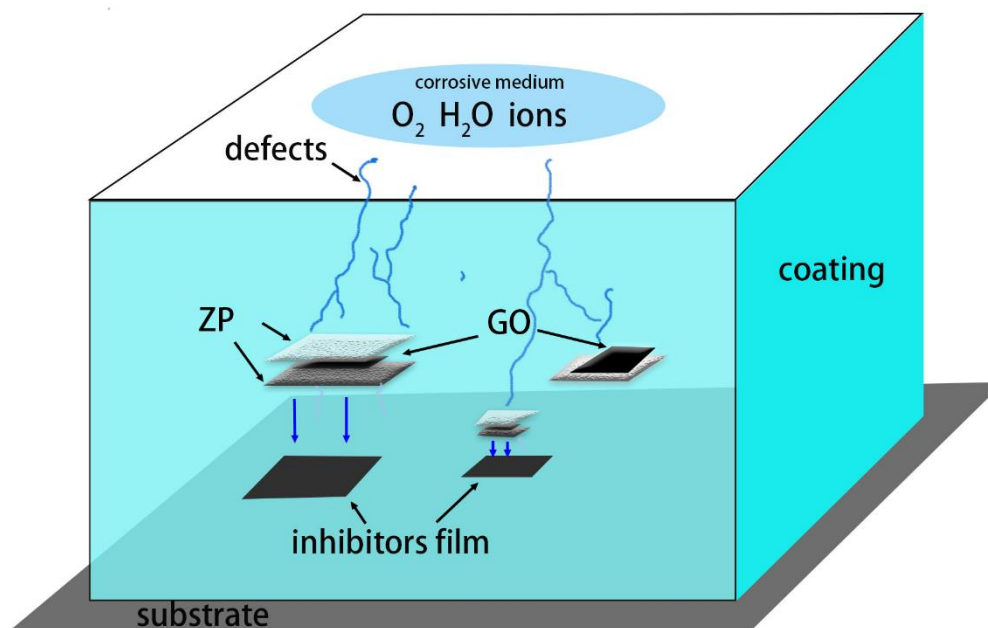


Figure 11. Schematic representation of the corrosion inhibition mechanism of the GO-ZP/WPU coating.

It can be seen from the data in Table 3 that the addition of GO resulted in an increase in the R_{ct} value of the GO-ZP composites compared with that of the zinc phosphate sample. The diameter of the semicircles increased in the sequence of steel < WPU < GO-ZP (3:1)-0.1wt% < GO-ZP (3:1)-1 wt% < ZP 0.5 wt% < GO-ZP (5:1)-0.5 wt% < GO-ZP (1:1)-0.5 wt% < GO-ZP (3:1)-0.5 wt% coating, which indicated that the prepared composites obtained good anticorrosive performance when they had a suitable ratio. In addition, the R_{ct} value for GO-ZP (3:1)-0.5 wt% ($1.104 \times 10^4 \Omega \text{ cm}^2$) coating increased the most and was 3 times larger than that of the zinc phosphate ($3.762 \times 10^3 \Omega \text{ cm}^2$) coating only. Although a further increase in GO content reduced the value of R_{ct} , the value for the GO-ZP (5:1) ($4.726 \times 10^3 \Omega \text{ cm}^2$) coating remained nearly twice as large as the pure WPU ($8.26 \times 10^2 \Omega \text{ cm}^2$) coating. Since phosphate is an insulator, it does not directly participate in the electrochemical corrosion reaction, and the added graphene oxide did not alter the corrosion protection mechanism of phosphate. The results of the potentiodynamic polarization curves and EIS measurements revealed that GO-ZP composites were very effective as anticorrosive reinforcements in the WPU coatings. This can be attributed to the graphene oxide acting as a deposition bed to accelerate phosphate deposition and provide an additional barrier in the film. The modification of zinc phosphate by graphene oxide drove the corrosion potential to move in the positive direction in the anticorrosive system. When the content of graphene oxide exceeded the appropriate proportion, the corrosion rate of the coating was affected and exhibited an upward trend. This result might be ascribed to the poor dispersion and restacking of the GO in the PU resin.

4. CONCLUSION

GO-ZP composites were successfully prepared by a one-step ultrasonic wave-assisted precipitation method and further used as a functional reinforcement to enhance the anticorrosive properties of a WPU coating and improve the anticorrosion efficiency of pure zinc phosphate. The zinc phosphate in the sandwich structure compensated for the surface defects of graphene caused by ultrasonication, and the zinc phosphate itself also formed an inhibitor film on the substrate. The introduction of graphene as a modifier in the system influenced the open circuit potential to have a positive shift and clearly reduced the corrosion tendency of the substrate. The results indicated that the corrosion resistance of the synthesized composites was closely related to the addition ratio of the composites in the coating and the mass ratio of GO to $Zn_3(PO_4)_2$. SEM images indicated that the particle size of the sample decreased as the content of GO increased, which improved the dissolution of zinc phosphate and increased the corrosion resistance. Moreover, electrochemical studies suggested that GO-ZP (3:1)-0.5 wt% composites had the best anticorrosion properties with the lowest corrosion current density ($4.41 \times 10^{-7} \text{ A/cm}^2$) and the maximum coating resistance ($1.104 \times 10^4 \text{ } \Omega \text{ cm}^2$). The data showed that the GO-ZP/WPU composite coating had a better corrosion resistance at a thinner film thickness, compared with RSG/WPU ($1.11 \times 10^{-6} \text{ A/cm}^2$) [24]. The GO-ZP/WPU composite coating was prepared using simpler steps compared with those to prepare the GO/phosphate coating ($R_{ct} = 2023 \pm 28 \text{ } \Omega \text{ cm}^2$) [35]. The above results showed that GO-ZP composites exhibit better corrosion protection than traditional zinc phosphate.

References

1. C. Yun, Y. Hao, H. Wei, J. Yan, W. Yang, X. Yin, L. Ying and L. Xiang, *Surf. Coat. Technol.*, 310 (2017) 122-128.
2. K. C. Chang, T. L. Chuang, W. F. Ji, C. H. Chang, H. Shih, C. L. Hsu, J. M. Yeh, W. C. Tang and Y. C. Su, *eXPRESS Polym. Lett.*, 9 (2015) 143-153.
3. Z. Yang, L. Wang, S. Wen, S. Li, T. Zhu, L. Wei and G. Liu, *Appl. Surf. Sci.*, 401 (2017) 146-155.
4. Ş. Erdoğan, Z. S. Safi, S. Kaya, D. Ö. Işın, G. Lei and C. Kaya, *J. Mol. Struct.*, 1134 (2017) 751-761.
5. B. Ramezanzadeh, Z. Haeri and M. Ramezanzadeh, *Chem. Eng. J.*, 303 (2016) 511-528.
6. N. A. A. Ghany, M. F. Shehata, R. M. Saleh and A. A. E. Hosary, *Mater. Corros.*, 68 (2017).
7. M. S. Gaikwad, V. V. Gite, P. P. Mahulikar, D. G. Hundiwale and O. S. Yemul, *Prog. Org. Coat.*, 86 (2015) 164-172.
8. K. D. Chattopadhyay, R. A. J. U. and V. S. N. K., *Prog. Polym. Sci.*, 32 (2007) 352-418.
9. T. Gurunathan, C. R. K. Rao, R. Narayan and K. V. S. N. Raju, *Prog. Org. Coat.*, 76 (2013) 639-647.
10. G. Liu, G. Wu, C. Jian and Z. Kong, *Prog. Org. Coat.*, 101 (2016) 461-467.
11. B. Ramezanzadeh, A. Ahmadi and M. Mahdavian, *Corros. Sci.*, 109 (2016) 182-205.
12. C. H. Chang, T. C. Huang, C. W. Peng, T. C. Yeh, H. I. Lu, W. I. Hung, C. J. Weng, T. I. Yang and J. M. Yeh, *Carbon*, 50 (2012) 5044-5051.
13. B. P. Singh, B. K. Jena, S. Bhattacharjee and L. Besra, *Surf. Coat. Technol.*, 232 (2013) 475-481.
14. O. C. Compton, S. Kim, C. Pierre, J. M. Torkelson and S. T. Nguyen, *Adv. Mater.*, 22 (2010) 4759-4763.
15. H. Kim, Y. Miura and C. W. Macosko, *Chem. Mater.*, 22 (2010) 3441-3450.

16. N. Yousefi, M. M. Gudarzi, Q. Zheng, X. Lin, X. Shen, J. Jia, F. Sharif and J.-K. Kim, *Composites, Part A*, 49 (2013) 42-50.
17. Y. Li, Z. Yang, H. Qiu, Y. Dai, Q. Zheng, J. Li and J. Yang, *J. Mater. Chem. A*, 2 (2014) 14139-14145.
18. Y. H. Yang, L. Bolling, M. A. Priolo and J. C. Grunlan, *Adv. Mater.*, 25 (2013) 503-508.
19. S. Qiu, W. Li, W. Zheng, H. Zhao and L. Wang, *ACS Appl. Mater. Interfaces*, 9 (2017) 34294-34304.
20. L. Guo, L. Jing, Y. Liu, B. Zou, S. Hua, J. Zhang, D. Yu, S. Wang, S. Wang and L. Wang, *Int. J. Electrochem. Sci.*, 13 (2018) 11867-11881.
21. H. Wang, Y. He, G. Fei, C. Wang, Y. Shen, K. Zhu, L. Sun, N. Rang, D. Guo and G. G. Wallace, *Chem. Eng. J.*, 359 (2019) 331-343.
22. Y.-H. Yu, Y.-Y. Lin, C.-H. Lin, C.-C. Chan and Y.-C. Huang, *Polym. Chem.*, 5 (2014) 535-550.
23. H. Kim, D. W. Kim, V. Vasagar, H. Ha, S. Nazarenko and C. J. Ellison, *Adv. Funct. Mater.*, 28 (2018) 1803172.
24. J. Luo, J. Wang, S. Wen, D. Yu, Y. Wu and K. Sun, *J. Coat. Technol. Res.*, 15 (2018) 1107-1115.
25. X. Luo, S. Yuan, X. Pan, C. Zhang, S. Du and Y. Liu, *ACS Appl. Mater. Interfaces*, 9 (2017) 18263-18275.
26. M. Choucair, P. Thordarson and J. A. Stride, *Nat. Nanotechnol.*, 4 (2009) 30.
27. J. Huang, X. Fu and Q. Miao, *Appl. Catal., A*, 407 (2011) 163-172.
28. N. Van Phuong, K. Lee, D. Chang, M. Kim, S. Lee and S. Moon, *Met. Mater. Int.*, 19 (2013) 273-281.
29. E. Alibakhshi, A. Naeimi, M. Ramezanzadeh, B. Ramezanzadeh and M. Mahdavian, *J. Alloys Compd.*, 762 (2018) 730-744.
30. A. Di Giampaolo, M. Medina, R. Reyes and M. Velez, *Surf. Coat. Technol.*, 89 (1997) 31-37.
31. X. Ding, L.-f. Xue, X.-c. Wang, K.-h. Ding, S.-l. Cui, Y.-c. Sun and M.-s. Li, *J. Magn. Magn. Mater.*, 416 (2016) 247-255.
32. E. Alibakhshi, E. Ghasemi and M. Mahdavian, *Corros. Sci.*, 77 (2013) 222-229.
33. E. Alibakhshi, E. Ghasemi and M. Mahdavian, *J. Sol-Gel Sci. Technol.*, 72 (2014) 359-368.
34. O. Dagdag, A. El Harfi, A. Essamri, A. El Bachiri, N. Hajjaji, H. Erramli, O. Hamed and S. Jodeh, *Arabian J. Sci. Eng.*, (2018) 1-11.
35. Y. Xie, M. Chen, D. Xie, L. Zhong and X. Zhang, *Corros. Sci.*, 128 (2017) 1-8.
36. W. S. Hummers Jr and R. E. Offeman, *J. Am. Chem. Soc.*, 80 (1958) 1339-1339.
37. S. Karekar, B. Bhanvase, S. Sonawane, M. Deosarkar, D. Pinjari and A. Pandit, *Chem. Eng. Process.*, 87 (2015) 51-59.
38. A. Samadi-Maybodi and S. K. H. Nejad-Darzi, *J. Iran. Chem. Soc.*, 9 (2012) 431-439.
39. A. J. Jadhav, D. V. Pinjari and A. B. Pandit, *Chem. Eng. J.*, 297 (2016) 116-120.
40. D. Yu, S. Wen, J. Yang, J. Wang, Y. Chen, J. Luo and Y. Wu, *Surf. Coat. Technol.*, 326 (2017) 207-215.
41. M. Crobu, A. Rossi, F. Mangolini and N. D. Spencer, *Anal. Bioanal. Chem.*, 403 (2012) 1415-1432.
42. D. Zhang, Y. Zhao and L. Chen, *Appl. Surf. Sci.*, 458 (2018) 638-647.
43. X. Zhou, H. Bai, H. Ma, H. Li, W. Yuan, H. Du, P. Zhang and H. Xin, *Mater. Character.*, 108 (2015) 22-28.
44. X. Zhou, H. Du, H. Ma, L. Sun, R. Cao, H. Li and P. Zhang, *J. Phys. Chem. Solids*, 78 (2015) 1-7.
45. R. Nie, J. Shi, S. Xia, L. Shen, P. Chen, Z. Hou and F.-S. Xiao, *J. Mater. Chem.*, 22 (2012) 18115-18118.
46. Y.-L. Chen, Z.-A. Hu, Y.-Q. Chang, H.-W. Wang, Z.-Y. Zhang, Y.-Y. Yang and H.-Y. Wu, *J. Phys. Chem. C*, 115 (2011) 2563-2571.
47. E. J. M. Edralin, J. L. Garcia, F. M. dela Rosa and E. R. Punzalan, *Mater. Lett.*, 196 (2017) 33-36.
48. C.-L. Yu, C. Y. Jimmy, H.-B. He and W.-Q. Zhou, *Rare Met.*, 35 (2016) 211-222.
49. S. L. Hem, *Ultrasonics*, 5 (1967) 202-207.

50. G. Ruecroft, D. Hipkiss, T. Ly, N. Maxted and P. W. Cains, *Org. Process Res. Dev.*, 9 (2005) 923-932.
51. H. Liu, T. Gu, G. Zhang, Y. Cheng, H. Wang and H. Liu, *Corros. Sci.*, 102 (2016) 93-102.

© 2019 The Authors. Published by ESG (www.electrochemsci.org). This article is an open access article distributed under the terms and conditions of the Creative Commons Attribution license (<http://creativecommons.org/licenses/by/4.0/>).